Available online at www.sciencedirect.com
SCIENCE DIRECT®
Journal of Solid State Chemistry 178 (2005) 3547–3553
JOURNAL OF SOLID STATE CHEMISTRY
www.elsevier.com/locate/jssc

A comparison of the structure and localized magnetism in Ce_2PdGa_{12} with the heavy fermion $CePdGa_6$

Robin T. Macaluso[a], Jasmine N. Millican[a], Satoru Nakatsuji[b], Han-Oh Lee[c], B. Carter[d], Nelson O. Moreno[d], Zachary Fisk[c], Julia Y. Chan[a,*]

[a]*Department of Chemistry, Louisiana State University, Baton Rouge, LA 70803, USA*
[b]*Department of Physics, Kyoto University, Kyoto, Japan 606-8502*
[c]*Department of Physics, University of California, Davis, CA 95616, USA*
[d]*Los Alamos National Laboratory, Los Alamos, NM 87545, USA*

Received 16 May 2005; received in revised form 8 September 2005; accepted 11 September 2005
Available online 10 October 2005

Abstract

Single crystals of Ce_2PdGa_{12} have been synthesized in Ga flux and characterized by X-ray diffraction. This compound crystallizes in the tetragonal $P4/nbm$ space group, $Z = 2$ with lattice parameters of $a = 6.1040(2)$ Å and $c = 15.5490(6)$ Å. It shows strongly anisotropic magnetism and orders antiferromagnetically at $T_N \sim 11$ K. A field-induced metamagnetic transition to the ferromagnetic state is observed below T_N. Structure–property relationships with the related heavy-fermion antiferromagnet $CePdGa_6$ are discussed.

Keywords: Heavy fermion; Metamagnet; $CePdGa_6$; Ce_2PdGa_{12}; Single crystal; Intermetallics

1. Introduction

Ce-based intermetallic compounds have attracted interest because of their variety of electronic properties. Extensive studies have been performed to understand so called "heavy fermion" states at low temperatures where large values of magnetic susceptibility and electronic specific heat are observed as a result of *f*-electrons coupling with conduction electrons [1]. The search for new layered materials is important in exploring new heavy fermion superconductors and in deepening our understanding of the role of structural dimensionality. This is indeed the case for the highest T_c to date, of a Ce-based heavy fermion superconductor, which is found in the layered $CeCoIn_5$ ($T_c = 2.3$ K) [2].

We have previously reported the synthesis and structure of a new Ce-based layered intermetallic compound, $CePdGa_6$, and its La-analog [3]. $CePdGa_6$ exhibits heavy fermion behavior with a specific heat coefficient $\gamma \sim 230$–400 mJ/mol-Ce K^2. It shows highly anisotropic magnetism and orders antiferromagnetically at $T_N \sim 5.5$ K. The layered nature of the crystal structure, consisting of face-sharing $CeGa_{8/4}$ and edge-sharing $PdGa_{8/2}$ rectangular prisms alternating in a 1:1 ratio along the *c*-axis, is consistent with anisotropy observed in the magnetism. In the $CeGa_{8/4}$ layers, Ce is coordinated to 8 Ga atoms at the corners of rectangular prisms, forming face-sharing rectangular prisms. Meanwhile, the $PdGa_{8/2}$ layers consist of edge-sharing rectangular prisms with Pd at the center and Ga atoms at the corners.

In our search for new layered materials in ternary Ce–Pd–Ga system, we have discovered a new phase, Ce_2PdGa_{12}. The tetragonal structure is composed of Ce–Ga and $PdGa_{8/2}$ layers, similar to $CePdGa_6$. Magnetic and specific heat measurements suggest an antiferromagnetic (AF) ground state of Ce_2PdGa_{12}, whose spin configuration transforms from a collinear AF to a canted one on lowering temperature. Moreover, we have found a field-induced metamagnetic transition in the AF state. We will discuss the structure–property relationships with the related heavy-fermion antiferromagnet $CePdGa_6$.

*Corresponding author. Fax: +225 578 3458.
E-mail address: jchan@lsu.edu (J.Y. Chan).

0022-4596/$ - see front matter © 2005 Elsevier Inc. All rights reserved.
doi:10.1016/j.jssc.2005.09.013

2. Experimental

2.1. Synthesis

Single-phase crystals of La_2PdGa_{12} and Ce_2PdGa_{12} were obtained by using flux growth methods. La or Ce ingot (3N, Ames Laboratory), Pd (5N, Alfa Aesar), and Ga (5N, Alfa Aesar) were placed into an alumina crucible in a 1:1:20 ratio. The contents were sealed into an evacuated fused silica tube, and the ampoule was heated to 1423 K for 2 h and allowed to cool to 723 K at a rate of 8 K/h, at which point the ampoules were immediately inverted and spun with a centrifuge. Plate-like single crystals were mechanically extracted. Typical crystal size ranged between 0.125 and 1 cm^3. No noticeable degradation of the crystals in air was observed.

Single-phase crystals of $LaPdGa_6$ and $CePdGa_6$ were obtained by similar methods. La or Ce ingot (3N, Ames Laboratory), Pd (5N, Alfa Aesar), and Ga (5N, Alfa Aesar) were placed into an alumina crucible in a 1:1.5:15 ratio. After sealing the contents into a fused silica tube, the ampoule was heated at 1423 K for 2 h and allowed to cool quickly to 773 K at a rate of 150 K/h. The samples were then slow cooled at a rate of 8 K/h to 673 K, at which point the ampoules were immediately inverted and spun with a centrifuge. Single crystals were mechanically extracted. Flux growth methods using a 1:1:20 ratio of Ce:Pd:Ga and a heat treatment up to 1423 K followed by cooling at a rate of 8 K/h and centrifugation at 623 K yielded a mixture of $CePdGa_6$ and Ce_2PdGa_{12}.

2.2. X-ray diffraction

A suitable $0.03 \times 0.03 \times 0.08\,mm^3$ silver-colored fragment of Ce_2PdGa_{12} was mounted onto the goniometer of a Nonius KappaCCD diffractometer equipped with MoK_α radiation ($\lambda = 0.71073$ Å). Data were collected up to $\theta = 30.0^\circ$ at 293 K. A similar treatment was applied to a $0.05 \times 0.08 \times 0.08\,mm^3$ silver-colored fragment of La_2PdGa_{12}. Further crystallographic parameters for Ce_2PdGa_{12} and its La analog are provided in Table 1. The space group and atomic positions from Sm_2NiGa_{12} were used as an initial structural model for the structure determination of both La_2PdGa_{12} and Ce_2PdGa_{12} compounds. The structural model was refined using SHELXL97 [4]. Data were corrected for extinction and refined with anisotropic displacement parameters. Data were also corrected for absorption by a multi-scan method using HKL Scalepack. Atomic positions and displacement parameters for both compounds are provided in Table 2, and selected interatomic distances are provided in Table 3. To ensure homogeneity and sample quality, single-crystal X-ray diffraction was performed on several single crystals from multiple batches of samples. Single-crystal X-ray diffraction experimental results are consistent with the temperature schemes to obtain single-phase $CePdGa_6$ and Ce_2PdGa_{12}.

Table 1
Crystallographic parameters of La_2PdGa_{12} and Ce_2PdGa_{12}

Crystal data		
Formula	La_2PdGa_{12}	Ce_2PdGa_{12}
a (Å)	6.1080(6)	6.1040(2)
c (Å)	15.5540(9)	15.5490(9)
V (Å^3)	580.28(9)	579.64(5)
Z	2	2
Crystal dimension (mm^3)	$0.05 \times 0.08 \times 0.08$	$0.03 \times 0.03 \times 0.08$
Crystal system	Tetragonal	Tetragonal
Space group	$P4/nbm$	$P4/nbm$
θ range(°)	2.62–30.00	2.62–29.97
μ (mm^{-1})	50.582	50.906
Data collection		
Measured reflections	1474	1537
Independent reflections	483	487
Reflections with $I > 2\sigma(I)$	366	387
R_{int}	0.0626	0.0419
h	$-8 \rightarrow 8$	$-8 \rightarrow 8$
K	$-6 \rightarrow 6$	$-6 \rightarrow 6$
L	$-21 \rightarrow 17$	$-21 \rightarrow 21$
Refinement		
[a]$R_1[F^2 > 2\sigma(F^2)]$	0.0415	0.0380
[b]w$R_2(F^2)$	0.1030	0.1064
Reflections	483	487
Parameters	26	26
$\Delta\rho_{max}$ (eÅ^{-3})	2.925	3.778
$\Delta\rho_{min}$ (eÅ^{-3})	−1.618	−2.375

[a] $R_1 = \sum||F_o|-|F_c||/\sum|F_o|$.
[b] $wR_2 = [\sum[w(F_o^2-F_c^2)^2]/\sum[w(F_o^2)^2]]^{1/2}$.

Table 2
Atomic positions and displacement parameters in La_2PdGa_{12} and Ce_2PdGa_{12}

Atom	Wyckoff position	x	y	z	U_{eq} (Å^2)[a]
La	4*h*	3/4	1/4	0.2465(5)	0.0105(3)
Pd	2*c*	3/4	1/4	0	0.0105(3)
Ga1	4*g*	3/4	3/4	0.1840(1)	0.0170(4)
Ga2	4*g*	3/4	3/4	0.3418(1)	0.0134(4)
Ga3	8*m*	0.5004(2)	0.0004(2)	−0.0877(7)	0.0135(4)
Ga4	8*m*	0.5704(2)	0.0704(2)	0.4289(8)	0.0268(5)
Ce	4*h*	3/4	1/4	0.2466(4)	0.0098(3)
Pd	2*c*	3/4	1/4	0	0.0098(4)
Ga1	4*g*	3/4	3/4	0.1840(1)	0.0117(4)
Ga2	4*g*	3/4	3/4	0.3417 (9)	0.0149(4)
Ga3	8*m*	0.5003(1)	0.0003(1)	−0.0878(6)	0.0116(3)
Ga4	8*m*	0.5702(2)	0.0702(1)	0.4286(7)	0.0253(4)

[a] U_{eq} is defined as one-third of the trace of the orthogonalized U_{ij} tensor.

2.3. Physical property measurements

Magnetization data were obtained using a Quantum Design Magnetic Property Measurement System SQUID magnetometer. The temperature-dependent magnetization data were obtained first under zero-field cooled (ZFC)

Table 3
Selected interatomic distances (Å) of La_2PdGa_{12} and Ce_2PdGa_{12}

La_2PdGa_{12}		Ce_2PdGa_{12}	
La layer		*Ce layer*	
La–Ga1 (× 4)	3.2047(6)	Ce–Ga1 (× 4)	3.2033(5)
La–Ga4 (× 2)	3.2331(15)	Ce–Ga4 (× 2)	3.2286(13)
La–Ga3 (× 2)	3.2784(13)	Ce–Ga3 (× 2)	3.2772(11)
La–Ga3 (× 2)	3.2824(13)	Ce–Ga3 (× 2)	3.2808(11)
$PdGa_6$ segment		*$PdGa_6$ segment*	
Ga1–Ga3 (× 4)	2.6283(10)	Ga1–Ga3 (× 4)	2.6257(10)
Pd–Ga3 (× 4)	2.5570(13)	Pd–Ga3 (× 4)	2.5512(10)
(× 4)	2.5519(12)	(× 4)	2.5558(10)
Ga-only segment		*Ga-only segment*	
Ga2–Ga4 (× 4)	2.6204(11)	Ga2–Ga4 (× 4)	2.6173(10)
Ga4–Ga4 (× 1)	2.5260(3)	Ga4–Ga4 (× 1)	2.5290(2)

conditions from 2 to 330 K under a field of 0.1 T. Magnetization was then measured upon heating to obtain field-cooled (FC) data after cooling to 2 K under field. Field (H)-dependent measurements were collected at 2 K with H swept between 0 and 5.5 T. These procedures were followed for crystallographic *ab*-plane of the crystal aligned parallel and perpendicular to the magnetic field. The specific heat was measured by a thermal relaxation method from 20 to 0.35 K at zero magnetic field and ambient pressure using a Quantum Design Physical Property Measurement system. The entropy was obtained by integrating the specific heat divided by the temperature with respect to the temperature.

3. Results and discussion

3.1. Structure

The structure of Ce_2PdGa_{12} is shown in Fig. 1 and is isostructural to Sm_2NiGa_{12} [5]. Single crystals of Ce_2PdGa_{12} crystallize in the tetragonal space group, $P4/nbm$ (No. 125 with origin choice 2), $Z = 2$. The Ce, Pd, Ga1, Ga2, Ga3, and Ga4 atoms occupy the 4*h*, 2*c*, 4*g*, 4*g*, 8*m*, and 8*m* sites, respectively.

The structure can be viewed as Ce atoms residing in Ga cavities of a three-dimensional network of [PdGa]. The [PdGa] subunit can then be further divided into $PdGa_6$ segments and Ga-only segments. Within the $PdGa_6$ segment, there are slightly distorted $PdGa_{8/2}$ rectangular prisms, where the Pd atom is coordinated to eight Ga atoms: four Ga3 atoms with interatomic distances of 2.5512(10) Å and four other Ga3 atoms by 2.5558(10) Å. These distances are typical of Pd–Ga bonds in Pd_5Ga_3 [6], $PdGa_5$, Pd_2Ga [7], and in $CePdGa_6$ [3] where the bonding distances range between 2.388 and 2.701 Å. In addition, the sum of the two covalent radii of Ga (1.25 Å) and Pd (1.28 Å) is 2.53 Å [8], which is close to our experimental

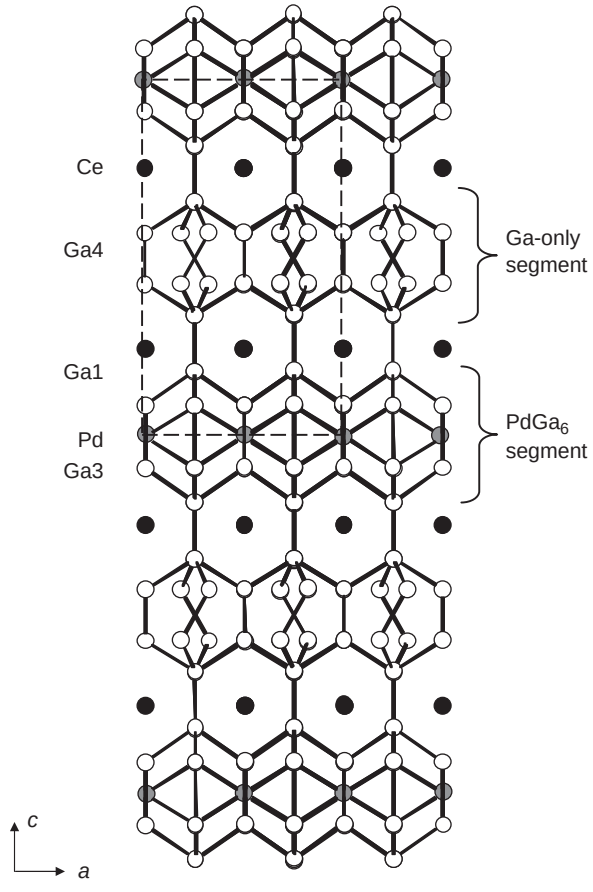

Fig. 1. The crystal structure of Ce_2PdGa_{12} along the *c*-axis is shown with Ce as black-filled circles, Pd as gray-filled circles, and Ga as white circles. The structure can be viewed as Ce contained in Ga cavities alternating with Ga-only segments and $PdGa_6$ segments. Dashed lines represent the unit cell.

Pd—Ga distances in Ce_2PdGa_{12}. The Ga3–Ga3 interatomic distance along the *ab*-plane is 3.0501(9) Å, too long to be considered a bond according to the 1.25 Å covalent

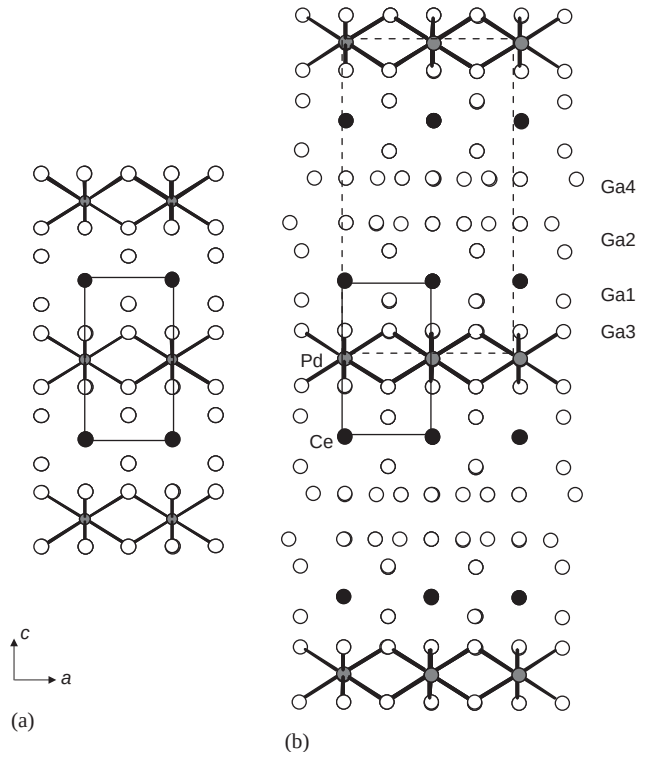

Fig. 2. The crystal structure of (a) $CePdGa_6$ and (b) Ce_2PdGa_{12}, is shown along the *c*-axis. Ce_2PdGa_{12} can be viewed as unit cells of $CePdGa_6$ alternating with Ga2 and Ga4 sheets along the *c*-axis. Black-filled circles represent Ce atoms, gray-filled circles represent Pd atoms, and white-filled circles represent Ga atoms. The solid and dashed lines represent the unit cell of $CePdGa_6$ and Ce_2PdGa_{12}, respectively.

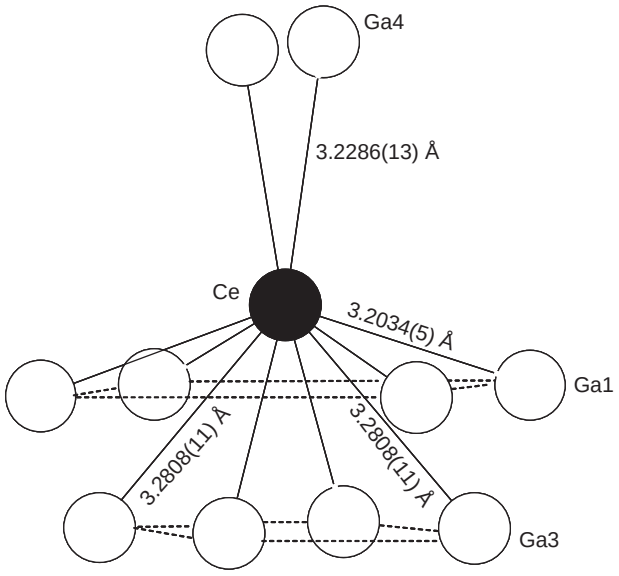

Fig. 3. The local Ce environment is shown. Ce caps a rectangular antiprism composed of Ga1 and Ga3 atoms. The dashed lines serve as a guide for the eye.

radius of Ga [8]. These distances in the $PdGa_{8/2}$ rectangular prisms are similar to the $PdGa_{8/2}$ prisms in $CePdGa_6$ where the Ga–Ga interatomic distance is shorter along the *c*-axis (2.7299(19) Å) and longer across the *ab*-plane (3.076(1) Å.).

To illustrate the striking resemblance between the two structures, the structure of $CePdGa_6$ and the structure of Ce_2PdGa_{12}, are presented in Fig. 2. The unit cell of $CePdGa_6$, which is shown as solid lines in Fig. 2a, can be viewed as a primitive unit cell with Ce at the origin. Pd atoms bisect each of the edges along the *c*-axis, and two Ga layers—each consisting of either Ga1 or Ga3—separate the Ce and Pd atoms. Fig. 2b shows that there is a similar packing arrangement found in Ce_2PdGa_{12}. In fact, Ce_2PdGa_{12} can be viewed as $CePdGa_6$ units (shown as solid lines) alternating with a Ga-only segment along the *c*-axis.

The Ga-only segment consists of two Ga layers; one layer is composed of Ga2 and the other of Ga4. The Ga2 sheet includes Ga2–Ga2 contact distances ranging between 4.3176(3) and 6.1060(4) Å, indicating that the Ga2 atoms are isolated from each other. The Ga4–Ga4 atoms, however, are separated by 2.5290(2) Å, similar to 2.50 Å, the bonding distance by summing two Ga covalent radii (1.25 Å) [8]. Ga4 atoms also form interatomic distances of 2.6173(10) Å with Ga2 atoms, falling within the range of 2.297–2.930 Å found in $CeGa_6$ [9], $CeGa_2$ [9], and $PdGa_5$ [7].

Fig. 3 shows the local Ce coordination of Ce_2PdGa_{12}. Using a Ce–Ga bonding cutoff of ~3.3 Å, which is larger than the projected sum of 2.9 Å of the Ce (1.65 Å) and Ga (1.25 Å) covalent radii [8], the Ce atom is coordinated to 10 Ga atoms: 4 Ga1, 4 Ga3, and, 2 Ga4 whereas Ce is coordinated to 8 Ga atoms in $CePdGa_6$. All of these Ce–Ga distances are similar to Ce–Ga bond distances found in the binary compounds, $CeGa_2$ [9] and $CeGa_6$ [9], which range between 3.252 and 3.299 Å. As shown in Fig. 3, the Ce atom caps a rectangular antiprism composed of Ga1 and Ga3 atoms. The Ce–Ga1 and Ce–Ga3 distances are 3.2034(5) Å (4 ×) and 3.2772(11) Å (4 ×), respectively. In addition, Ce is also bonded to two Ga4 atoms with an interatomic distance of 3.2286(13) Å. Rare-earth atoms can be found as the cap of main group layers, such as in $CeNiSb_3$ [3,10], $(RE)In_{1-x}Sb_2$ (RE = La–Nd) [11], $(RE)MSb_3$ (M = V, Cr) [12], and $RESb_2$ [13,14]. The Ga1 and Ga3 atoms surrounding Ce can be viewed as two different layers, where the Ga4 layer also serves as the face of the $PdGa_{8/2}$ rectangular prisms. Although the Ga1–Ga1 interatomic distance is greater than 4 Å and indicates that *intra*layer Ga1 interactions are unlikely, the distance between Ga1 and Ga3 layers of 2.6257(10) Å implies that there may be some weak *inter*layer interactions.

3.2. Magnetism

In order to compare the magnetic data of $CePdGa_6$ and Ce_2PdGa_{12}, we have re-measured the magnetization on single crystals of single-phase $CePdGa_6$ and Ce_2PdGa_{12}. Previous magnetic data of $CePdGa_6$ [3] apparently has a

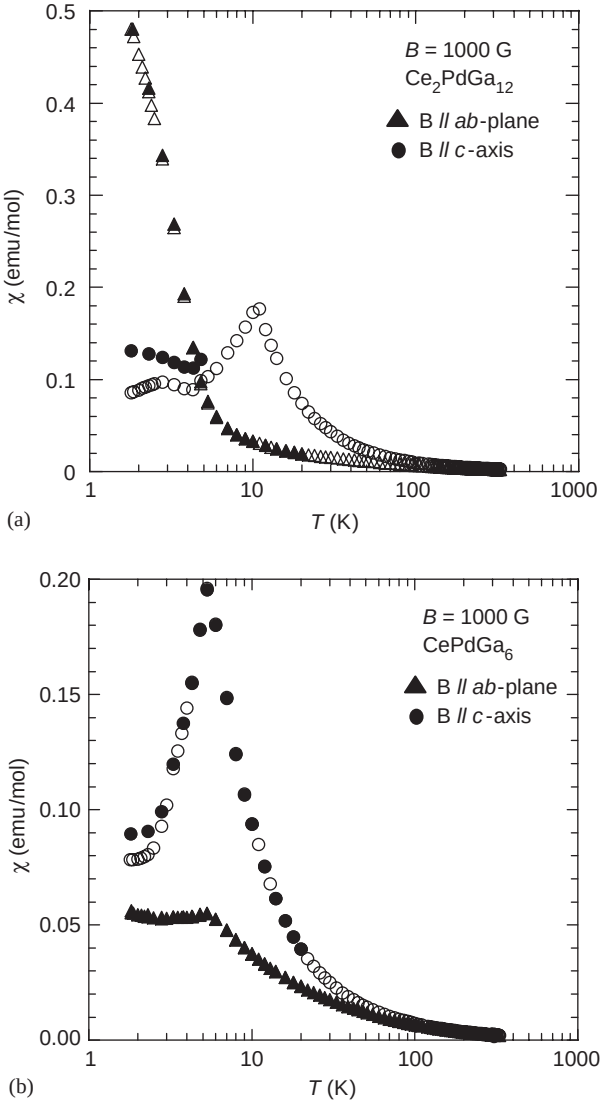

Fig. 4. Magnetic susceptibility (emu/mol Ce) as a function of temperature of (a) Ce_2PdGa_{12} and (b) $CePdGa_6$. Circles and triangles represent data for $B\|$crystallographic *ab*-plane and $B\|$crystallographic *c*-axis; open and closed symbols represent field-cooled and zero-field cooled data, respectively.

Ce_2PdGa_{12} inclusion. The temperature dependence of the susceptibility χ is given for Ce_2PdGa_{12} and $CePdGa_6$ in Figs. 4a and b, respectively. The field of 0.1 T was applied along *ab*-plane and *c*-axis. In Ce_2PdGa_{12}, data for both orientations follow Curie–Weiss behavior above 100 K. The effective moments, μ_{eff}, are estimated to be 2.54 μ_B (*ab*-plane) and 2.59 μ_B (*c*-axis), very similar to the expected Ce $J = 5/2$ local moment, $\mu_{eff} = 2.54\,\mu_B$, with $\theta = -14.8$ K (*ab*-plane) and 18.2 K (*c*-axis). While a clear cusp in the *c*-axis component at 11 K is indicative of an antiferromagnetic transition, the *ab*-plane component shows a steep increase below about 3 K. A broad peak is also observed at 3 K in the C_P/T vs. T plot. This suggests an appearance of a ferromagnetic component. This strong anisotropy is most likely due to the canting of spins in the Néel state below 11 K, creating a net ferromagnetic component along the

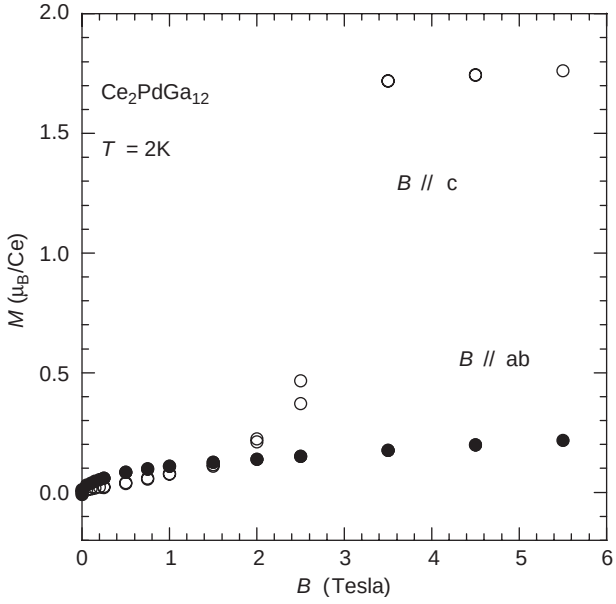

Fig. 5. Magnetization as a function of field with $B\|ab$-plane shown in black circles and $B\|c$-axis in white circles.

ab-plane. The susceptibility of La_2PdGa_{12} (not shown) shows non-magnetic behavior ($\chi = -10^{-4}$ emu/mol at 273 K), indicating that the magnetic moments result only from the Ce *f*-electron, not from Pd *d*-electrons. $CePdGa_6$, on the other hand, shows an antiferromagnetic transition at 5 K with the cusps in both the *ab*-plane and *c*-axis components. The Curie–Weiss analysis above 100 K yields the effective moments of $\mu_{eff} = 2.48\,\mu_B$ (*ab*-plane) and 2.45 μ_B (*c*-axis), with $\theta = -12.9$ K (*ab*-plane) and -1.17 K (*c*-axis), suggesting antiferromagnetic interactions. Single-crystal neutron diffraction experiments are in progress to determine the magnetic structures for $CePdGa_6$ and Ce_2PdGa_{12}.

The field dependence of the magnetization M for Ce_2PdGa_{12}, as shown in Fig. 5, was measured under fields along the *c*-axis and *ab*-plane. Interestingly, the *c*-axis magnetization shows a jump at 2.5 T, after showing a linear increase with the field. This indicates a metamagnetic transition, most likely due to a spin-flip transition from an antiferromagnetic to a ferromagnetic state. Along the crystallographic *ab*-plane, on the other hand, M increases rapidly up to $B = 1$ T and reaches the value $\sim 0.2\,\mu_B$ at 5 T. A small hysteresis is observed below 0.1 T at 2 K, indicating the system has a ferromagnetic component in the *ab*-plane. The field dependence is similar to $CePdGa_6$ [3] where the magnetization shows a jump at 2 T, lower than the metamagnetic transition of Ce_2PdGa_{12}.

3.3. Specific heat

As discussed in the synthesis section, we have established synthetic routes to obtain single-phase crystals for both $CePdGa_6$ and Ce_2PdGa_{12}. Their temperature dependences of the specific heat were measured and are shown in Fig. 6.

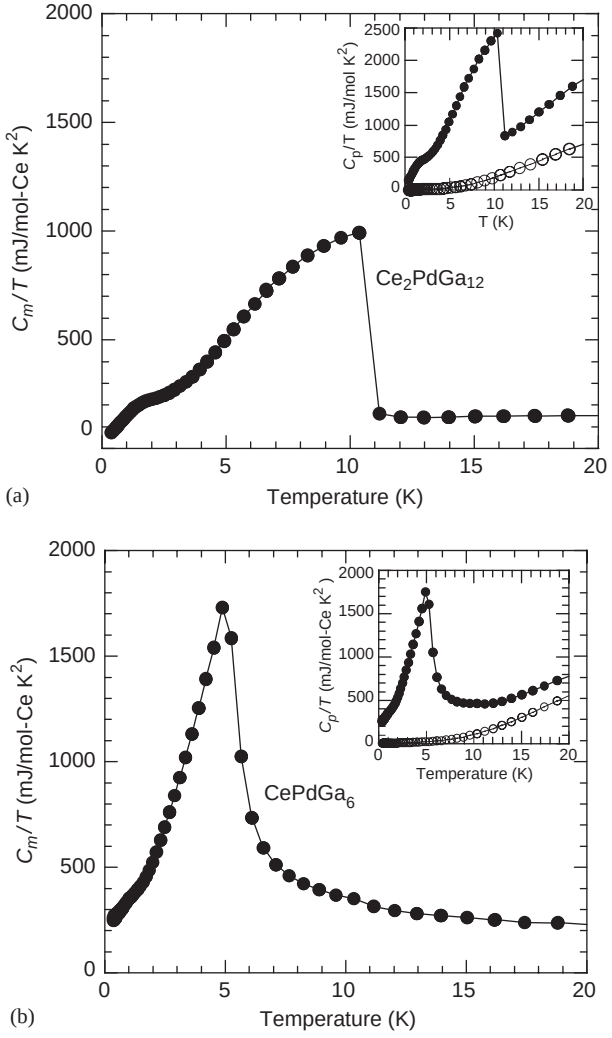

Fig. 6. The magnetic portion of the specific heat, C_m/T, of (a) Ce_2PdGa_{12} and (b) $CePdGa_6$ as a function of temperature are shown. The line serves as a guide for the eye. C_m/T is obtained by subtracting the heat capacity of the La-analog (shown as white circles in inset) from the total heat capacity of each respective compound (shown as black circles in inset).

There are small deviations in the data from our previous report on $CePdGa_6$ [3]. Because $CePdGa_6$ and Ce_2PdGa_{12} can coexist under a certain growth condition (see Section 2.1), the previous report on the specific heat and magnetism of $CePdGa_6$ has minor effects from the inclusion of Ce_2PdGa_{12} [3].

The magnetic part of the specific heat, C_m/T, for Ce_2PdGa_{12} (Fig. 6a) and $CePdGa_6$ (Fig. 6b) is estimated by subtracting the specific heat C_P/T of the La-analogue from the specific heat C_P/T of the Ce-compound. For clarity, we show C_P/T for both Ce and La-analogues in each inset of Fig. 4. A sudden jump at 11 K, coincident with its antiferromagnetic transition, is observed in the C_m/T of Ce_2PdGa_{12}. Similarly a peak is observed in the heat capacity is observed at the antiferromagnetic transition temperature of 5.5 K for $CePdGa_6$. C_m/T shows electronic specific heat coefficient γ of $\sim$72 mJ/mol K^2 at T close to 0 K and almost constant with $\sim$140 mJ/mol K^2 at $T > T_N$ for Ce_2PdGa_{12}, smaller than γ ($\sim$230–400 mJ/mol K^2) for $CePdGa_6$.

The corresponding entropies for the f-electron contribution can be estimated by integrating C_m/T for Ce_2PdGa_{12} and $CePdGa_6$. The entropy (S) released below T_N is about 6000 (mJ/mole-K) for Ce_2PdGa_{12}, while it is around 5000 (mJ/mole-K) for $CePdGa_6$. These values are roughly close to $R\ln 2$ ($\sim$5800 mJ/mole-K), which represents a doubly degenerate ground state in the paramagnetic regime. In addition, the suppressed entropy at T_N in $CePdGa_6$ is attributable to Kondo effect.

3.4. Structure–property relationships

Two distinct Ce–Ce distances represent the structure of both compounds: Ce–Ce distances along the *ab*-plane, $(Ce–Ce)_{ab}$, and *c*-axis, $(Ce–Ce)_c$. In $CePdGa_6$, the Ce–Ce interatomic distances are 4.350(3) Å in the *ab*-plane and 7.922(6) Å along the *c*-axis [3]. As for Ce_2PdGa_{12}, since Ce atoms separate $PdGa_{8/2}$ and Ga-only segments that stack along the *c*-axis, there are two distinct $(Ce–Ce)_c$ distances along the *c*-axis. Thus, the $(Ce–Ce)_{ab}$ interatomic spacing in Ce_2PdGa_{12} is 4.318(6) Å and $(Ce–Ce)_c$ distances measure 7.664(5) Å and 7.882(6) Å. For both compounds, one would expect the magnetic correlations in the *ab*-plane to be stronger than those along the *c*-axis.

Coupled with the comparable crystal structures and the similar Ce–Ce distances found in both compounds, $CePdGa_6$ and Ce_2PdGa_{12} are expected to share similar overall physical properties, that is, an antiferromagnetic ground state and metamagnetic transition under a field applied along the *c*-axis. On the other hand, there are still some differences between the two. The higher Néel temperature with ferromagnetic component and the smaller γ for Ce_2PdGa_{12} may result from the difference of the number of Pd in the unit cell.

Ce–Ce distances are longer than the Hill limit, suggesting that Ce f moments interact through RKKY (Ruderman–Kittel–Kasuya–Yosida) interactions by hybridizing with conduction electrons of surrounding Ga atoms. Hybridization also induces the Kondo effect that should suppress the Néel order by competing with RKKY interactions. Reduced entropy ($S\sim$5000 mJ/mole-K) at T_N in $CePdGa_6$, suggests that the Kondo effect is more pronounced in $CePdGa_6$, suppressing T_N further in comparison with Ce_2PdGa_{12}. However, the difference in the Ce–Ga hybridization should not be the main reason for the differences between the two compounds because the Ce–Ga interatomic distances are nearly the same for both compounds. Hence, it is likely that the Pd atoms affect the magnetic properties by providing carriers to the systems. Ce_2PdGa_{12} has one less Pd atom than "$Ce_2Pd_2Ga_{12}$" (obtained by doubling the chemical formula of $CePdGa_6$). Generally, the decrease in the carrier number should result in two effects: (1) more localized nature of 4f electrons because of lack of screening by conducting carriers, and (2) proximity to the ferromagnetic state through RKKY interactions.

The observed weaker Kondo effects along with ferromagnetic components in Ce_2PdGa_{12} are indeed consistent with the smaller number of carriers due to less Pd in comparison with $CePdGa_6$.

4. Conclusion

We have synthesized Ce_2PdGa_{12}, which has a structure closely related to $CePdGa_6$. Our magnetic and thermal measurements have revealed double magnetic transitions. An antiferromagnetic transition occurs at 11 K, while a ferromagnetic component in the *ab*-plane appears by means of a second transition at ~5 K. This metamagnetic transition is most likely due to a spin flop interaction. Comparing the structures and magnetic behavior with those for $CePdGa_6$, we argue that the *f*-electron state of Ce_2PdGa_{12} is more localized and close to a ferromagnetic state because the carrier density is decreased by the lack of Pd atoms. It would be interesting to further study the effects of layering and Pd carriers by synthesizing a compound such as "Ce_3PdGa_{18}". This insertion of Ga layers between each '$CePdGa_6$ layer' may allow us to tune the transition temperature further.

Crystallographic Information Available: Crystallographic information files are available for La_2PdGa_{12} and Ce_2PdGa_{12}.

Acknowledgments

This work was supported in part by the Alfred P. Sloan Award, NSF DMR-0237664 (J.Y.C.), and NSF DMR-9971348 (Z.F.). R. M. would also like to acknowledge GIAR Award, Sigma Xi. Work at Los Alamos National Laboratory was supported by the US Department of Energy.

This work was supported in part by Grants-in-Aids for Scientific Research from JSPS and for the 21st Century COE "Center for Diversity and Universality in Physics" from MEXT of Japan.

References

[1] Z. Fisk, D.W. Hess, C.J. Pethick, D. Pines, J.L. Smith, J.D. Thompson, J.O. Willis, Science 239 (1988) 33.
[2] C. Petrovic, P.G. Pagliuso, M.F. Hundley, R. Movshovich, J.L. Sarrao, J.D. Thompson, Z. Fisk, P. Monthoux, J. Phys.: Condens. Matter 13 (2001) L337.
[3] R.T. Macaluso, S. Nakatsuji, H. Lee, M. Moldovan, Z. Fisk, J.Y. Chan, J. Solid State Chem. 174 (2003) 296.
[4] G.M. Sheldrick, SHELXL97, University of Göttingen, Germany, 1997.
[5] X.Z. Chen, P. Small, S. Sportouch, M. Zhuravleva, P. Brazis, C.R. Kannewurf, M.G. Kanatzidis, Chem. Mater. 12 (2000) 2520.
[6] S. Bhan, H. Kudielka, Z. Metallkd. 69 (1978) 333.
[7] K. Schubert, H.L. Lukas, H.G. Meissner, S. Bhan, Z. Metallkd. 50 (1959) 534.
[8] J. Emsley, The Elements, Oxford University Press, New York, 1991.
[9] G. Kimmel, D. Dayan, A. Grill, J. Pelleg, J. Less-Common Met. 75 (1980) 133.
[10] R.T. Macaluso, D. Wells, R.E. Sykora, T.E. Albrecht-Schmitt, A. Mar, S. Nakatsuji, H. Lee, Z. Fisk, J.Y. Chan, J. Solid State Chem. 177 (2004) 293.
[11] M.J. Ferguson, R.E. Ellenwood, A. Mar, Inorg. Chem. 38 (1999) 4503.
[12] M. Brylak, W. Jeitschko, Z. Naturforsch. B: Chem. Sci. 50 (1995) 899.
[13] R. Wang, H. Steinfink, Inorg. Chem. 6 (1967) 1685.
[14] N.L. Eatough, H.T. Hall, Inorg. Chem. 8 (1969) 1439.